

Learning Spatiotemporal Features of Ride-sourcing Services with Fusion Convolutional Network

Dapeng Zhang^a, Feng Xiao^{a,*}, Lu Li^b, Gang Kou^a

^a*School of Business Administration, Southwestern University of Finance and Economics, Chengdu, China.*

^b*California PATH, University of California, Berkeley, Richmond, CA, United States.*

Abstract

In order to collectively forecast the demand of ride-sourcing services in all regions of a city, convolutional neural networks (CNNs) have been applied with commendable results. However, local statistical differences throughout the geographical layout of the city make the spatial stationarity assumption of the convolution invalid, which limits the performance of CNNs on demand forecasting task. Hence, we propose a novel deep learning framework called LC-ST-FCN (locally-connected spatiotemporal fully-convolutional neural network) that consists of a stack of 3D convolutional layers, 2D (standard) convolutional layers, and locally connected convolutional layers. This fully convolutional architecture maintains the spatial coordinates of the input and no spatial information is lost between layers. Features are fused across layers to define a tunable nonlinear local-to-global-to-local representation, where both global and local statistics can be learned to improve predictive performance. Furthermore, as the local statistics vary from region to region, the arithmetic-mean-based metrics frequently used in spatial stationarity situations cannot effectively evaluate the models. We propose a weighted-arithmetic approach to deal with this situation. Our findings are three-fold: (1) 3D convolutions are more suitable for spatiotemporal feature learning compared to 2D convolutions; And the locally connected convolutional layers can deal with the impact of local statistical differences well, better than fully connected layers or standard convolutional layers. (2) The weighted-arithmetic approach is able to eliminate the inconsistencies between the absolute and percentage errors, which makes the comparison of predictive performances among different models more convenient. (3) The aleatoric uncertainty arising from the data generating process, which is often neglected in deep learning models, has great influence on the final predictive performance of the model. In the experiments, a real dataset from a ride-sourcing service platform (DiDiChuxing) is used, which demonstrates the effectiveness and superiority of our proposed model and evaluation method.

Keywords:

3D convolution, Fusion, Locally-connected, Ride-sourcing, Spatiotemporal.

*Corresponding author

Email address: evan.fxiao@gmail.com (Feng Xiao)

1. Introduction

In recent years, ride-sourcing service platforms, such as DiDiChuxing, Uber, and Lyft, have developed rapidly worldwide, aided by the growth of mobile internet, location-based services, cloud computing, and other innovative technologies. These platforms have various advantages compared to taxis, which suffer from temporal-spatial imbalance between supply and demand (Vazifeh et al., 2018). Ideally, the unoccupied driving time of ride-sourcing services is much less than that of taxis, which alleviates road congestion, reduces pollution emissions, and results in lower costs for the driver and mileage charges for the passenger. However, a new report from the *San Francisco County Transportation Authority* showed that traffic congestion throughout the city increased from 2010 to 2016, where half of the congestion was attributed to the increase in ride hails (Jessica Christian, 2018) due to unoccupied driving time, finding parking spaces, and locating passengers.

Although the efficiency of matching drivers and passengers has been greatly improved by ride-sourcing services (Dong et al., 2018), short-term prediction of passenger demand are still highly important for ride-sourcing service platforms so that available vehicles can be transferred from low-demand to high-demand areas in advance. This can effectively improve overall travel efficiency by reducing the waiting times for passengers, reducing ineffective mileage for drivers, increasing the matching rate, and decreasing costs. Further optimization of the unoccupied driving time and accurate prediction of short-term travel demand are being aided by the development of electronic sensors and wireless communication technology, global positioning system (GPS), global mobile communication system (GSM), and WiFi. At present, most ride-sourcing vehicles are equipped with such devices, which provide rich spatial and temporal information of the vehicle. These data have been very useful for supply and demand forecasting, fleet dispatching, travel time estimation, and route planning (Chen et al., 2017b; Auer et al., 2017).

Various demand forecasting models have been developed up to date. Time series models are the most widely used methods, such as autoregressive integrated moving average model (ARIMA). Other machine learning methods have also been used, such as the deep neural network (DNN), the recurrent neural network (RNN), and convolutional neural network (CNN) models. Since the short-term demand forecasting models must consider both time and space, i.e., at a given time t , one must predict the demand in a certain region during the time period $[t, t + \Delta t]$, typical CNNs, including LeNet (LeCun et al., 1989), AlexNet (Krizhevsky, 2012), and its deeper successors (Simonyan and Zisserman, 2014b; Szegedy et al., 2015), cannot be used directly for demand forecasting problems. The detailed reasons are illustrated below:

(1) Time series statistics: In the case of demand forecasting problems, it is desirable to capture the time series statistics of demand for multiple adjacent time intervals. CNNs have been primarily applied to 2D feature maps to compute features only from spatial dimensions. Although typical CNNs can also take inputs with time dimension by arranging time series data in multiple channels, the temporal information is still collapsed completely after the first convolution layer (Simonyan and Zisserman, 2014a).

(2) Spatial coordinates: Typical CNNs ostensibly take fixed-sized inputs and produce non-spatial outputs as the fully connected layers have fixed dimensions and the spatial coordinates are lost (Shelhamer et al., 2014). For short-term passenger demand forecasting, detailed predictions in all regions of a city depend on both global and local features, which need to be encoded using the spatial coordinates.

(3) Parameter sharing scheme: By assuming spatial stationarity, the parameter sharing

scheme can be used in convolutional layers, which dramatically reduce the number of parameters. However, the spatial stationarity assumption does not hold in a city where the local statistics or features vary from region to region.

In order to address these problems, we develop LC-ST-FCN, a new CNN-based DL model to handle the unique challenges of short-term passenger demand forecasting. In LC-ST-FCN model, the 3D convolutional operations are used to capture the time series statistics, which have achieved great performance on various video analysis tasks (Karpathy et al., 2014; Shuiwang et al., 2013). Since 3D convolution is a natural extension of standard convolution, features from both spatial and temporal dimensions can be learned simultaneously. The overall architecture of the LC-ST-FCN is a fully convolutional network that takes input of arbitrary size and produces output of the same size; the spatial coordinates are maintained throughout the process and no spatial information is lost between layers. We fuse features across the layers to define a tunable nonlinear local-to-global-to-local representation where both global and local statistics are learned to improve the predictive performance.

For the demand forecasting problem of ride-sourcing services, which is essentially a regression problem, local differences in the statistics are critical for both the model structure and evaluation. We propose a weighted scheme to better compare different models. In addition, although the stationarity and randomness of data are seldom considered in DL models, we observe that the randomness arising from the data generating process leads to learning difficulties in some regions. Hence, we classify all regions into two categories based on their randomnesses and evaluate the effect of uncertainty in the data on the predictive performance of DL models in demand forecasting problems.

The remainder of the paper is organized as follows. Section 2 reviews the existing literature. Section 3 describes the LC-ST-FCN model in detail. Section 4 outlines the evaluation of the model; we introduce the experimental dataset and metrics frequently used to evaluate model performance, analyze the inconsistency among those metrics and propose an improved method. Section 5 concludes the study and proposes future research directions.

2. Literature review

Demand forecasting using spatial and temporal data collected by internet and mobile terminals has becoming a research hotspot in the field of transportation. Kaltenbrunner et al. (2010) used data from the community bicycle program *Bicing* in Barcelona to analyze the pattern of human mobility in urban areas, and ARMA model was used to predict the number of bicycles available at different sites. Moreira-Matias et al. (2013) used the ARIMA model to forecast the demand of different taxi stations in Porto and Portugal, while the Markov algorithm, Lempel-Ziv-Welch algorithm, passion model, Moran’s I values and others have been used to predict time-series data of traffic (Deng and Ji, 2011; Moreira-Matias et al., 2013; Zhao et al., 2016). Other studies used spatial clustering to mine taxi demand and GPS trajectory data, and studied the demand distribution of taxis in urban areas (Chang et al., 2009; Yuan et al., 2011).

In recent years, DL technology has made tremendous progress, and has been widely used in many fields, including advanced speech recognition, visual object recognition, object detection, drug discovery, and genomics (Lecun et al., 2015). DL can transform original information into a higher level with more abstract expression using a simple non-linear model. After sufficient combinations of transformations, very complex functions can be learned. Therefore, DL meth-

ods are being increasingly applied to traffic prediction problems. Huang et al. (2014) proposed a neural network model composed of a deep belief network (DBN) and a multitask regression layer to predict short-term traffic flow. Ma et al. (2015) developed a depth-limited Boltzmann machine and RNN architecture to simulate and predict the evolution of traffic congestion. Chen et al. (2017a) studied the travel behavior of ride-sourcing services using an ensemble method.

To realize accurate region-based forecasting, a number of deep learning models were designed to model the complex spatiotemporal information, and state-of-the-art results were achieved (Ke et al., 2017; Ma et al., 2017; Xingjian and Woo, 2015; Yao et al., 2018; Yu et al., 2017). Most of previous studies have focused on the combination of convolutional neural network and recurrent neural network, where the recurrent neural network architecture was utilized to model the temporal dependencies. The most related work to this paper is the model proposed by Zhang et al. (2017), in which the different components of temporal properties were learned separately and fused by a parametric-matrix-based method. Different from previous studies, the 3D convolution operations were employed to simultaneously capture the spatiotemporal dependencies in this paper. Other previous studies have also shown that 3D convolution operations have powerful ability to learn the spatiotemporal features (Tran et al., 2015; Hara et al., 2017). In particular, locally connected convolutional layers were used at the end of the model to obtain the final prediction results, without parameter sharing (Gregor and Lecun, 2010; Huang et al., 2012; Taigman et al., 2014). To avoid the loss of spatial information, all of these convolution layers were applied with appropriate padding (only spatial) and stride 1, thus there was no change in term of spatial size from the input to the output of these convolution layers. Thus, this fully convolutional architecture was able to maintains the spatial coordinates of the input and no spatial information was lost between layers (Shelhamer et al., 2014).

3. The LC-ST-FCN model

In this study, we partition a city into an $I \times J$ grid map based on the longitude and latitude, where a grid cell denotes a region. We divide the observation time period into n time intervals with the interval length Δt to produce set T , where $T = 1, 2, \dots, t, \dots, n$. During the period $[t, t + \Delta t]$, the order demand generated in the region (i, j) is $x_t^{(i,j)}$, and the demand matrix of the entire $I \times J$ region is $X \in \mathbb{R}^{I \times J \times T}$.

Our goal is to predict how many orders will emerge during the future period $[t, t + \Delta t]$ for each region at an instant t . That is, given the historical observations $\{X_t \mid t = 0, \dots, n - 1\}$, X_n is predicted. The LC-ST-FCN model shown in Figure 1 is developed to achieve this goal. We select a collection of short pieces from historical observations and stack them together to form a 3D volume as input. The 3D convolution operations are used to fusion the spatial and temporal information in multiple contiguous time windows. Since 3D convolution is a natural extension of standard convolution, features from both spatial and temporal dimensions can be learned simultaneously. Then, multiple 2D convolutional layers are used to extract and encode features from low to high level, and from local to global. With the increasing of network depth, the receptive field of neurons also increases, allowing an increasing amount of spatial information to be learned. In particular, locally connected convolutional layers are used at the end of the model to obtain the final prediction results, without parameter sharing.

According to the findings in 2D CNNs (Simonyan and Zisserman, 2014b), small receptive fields of 3×3 convolution kernels with deeper architectures yield best results. Hence, in our LC-ST-FCN model we fix the spatial receptive field to 3×3 and vary only the temporal depth of the 3D convolution kernels. The 3D convolution kernel has access to information across

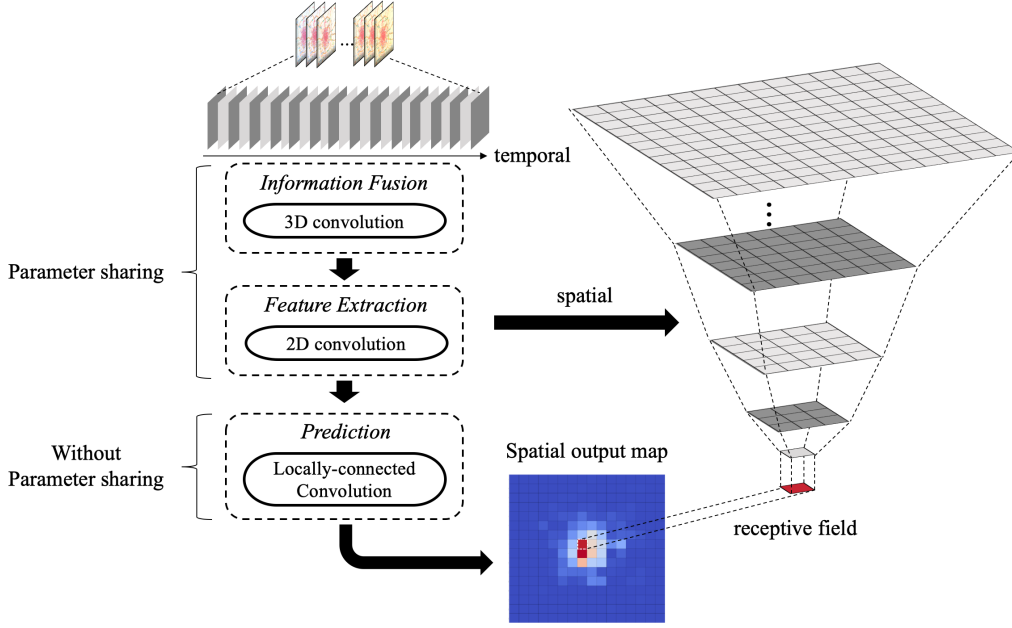


Figure 1: End-to-end implementation of the LC-ST-FCN model.

all input demand matrix after several layers, depending on the depth of the input data. The important components and training methods of the LC-ST-FCN model are introduced in the following sections.

3.1. Input: 3D volume

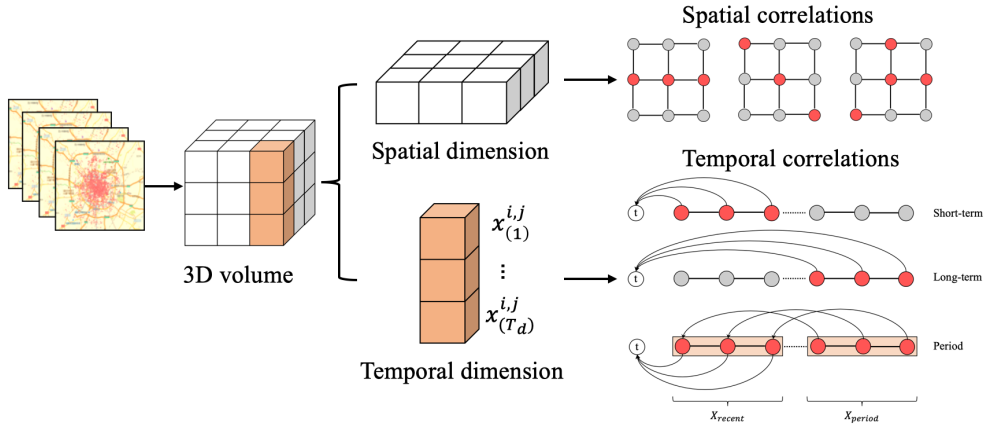


Figure 2: Schematic diagrams of the 3D volume of time series demand data.

As a class of attractive deep models for automated spatial feature construction, CNNs have been primarily applied on 2D images. However, for short-term passenger demand forecasting, it is also important to capture the temporal information in multiple adjacent or periodic time intervals. For example, there is a high demand for morning and evening rush-hour trips, but a low demand before dawn. Therefore, we construct the following input data forms, which integrate the spatiotemporal information of multiple time intervals into one 3D volume, with one demand matrix for each time interval:

$$X^{input} = [X_{recent}; X_{period}], X^{input} \in \mathbb{R}^{I \times J \times T_d} \quad (1)$$

$$X_{recent} = [X_{t-1}, \dots, X_{t-T_{recent}}], X^{input} \in \mathbb{R}^{I \times J \times T_{recent}} \quad (2)$$

$$X_{period} = [X_{t-L-1}, \dots, X_{t-L-T_{period}}], X^{input} \in \mathbb{R}^{I \times J \times T_{period}} \quad (3)$$

$$T_d = T_{recent} + T_{period} \quad (4)$$

Here, T_d , T_{recent} and T_{period} are the numbers of time intervals in X^{input} , X_{recent} and X_{period} separately. L is the periodic length of the demand time series data. The periodicity of travel demand is the sharing feature of urban activities, so we use an additive model (Brockwell and Davis, 2015) to determine the periodicity. Then, we decompose the overall travel demand X_t^{all} in the city into trend term X_t^{tre} , periodic term X_t^{per} , and residual term X_t^{res} :

$$X_t^{all} = \sum_i \sum_j x_t^{i,j}, t \in T \quad (5)$$

$$X_t^{res}(L) = X_t^{all} - X_t^{tre}(L) - X_t^{per}(L), 0 \leq L \leq T \quad (6)$$

$$L^* = \operatorname{argmin} X_t^{res}(L) \quad (7)$$

In the additive model, different X_t^{res} values can be obtained by choosing different L values, where smaller X_t^{res} values indicate that the corresponding L is closer to the practical situation. After T_{recent} , T_{period} and L are chosen, we can then construct the 3D volume, as shown in Figure 2. Each instance used by the LC-ST-FCN model is a 3D volume containing T_d number of raw samples with each sample represented by a matrix of $I \times J$ grid values.

3.2. The fusion of fully connected 3D and 2D Convolutions

In 2D CNNs, convolutions are applied on the 2D feature maps to compute features from the spatial dimensions only. When the 2D CNN is applied to demand forecasting problem, it is desirable to capture the temporal information in multiple time intervals, e.g. trend and period. Although 2D CNN can also take multiple time intervals as input, after the first convolution layer, temporal information is collapsed completely. Hence, it is difficult to effectively extract temporal information by 2D convolution operations. Compared to 2D convolution, 3D convolution has the ability to model temporal information better, owing to that 3D convolution preserves the temporal information of the input by maintaining a 3D volume as the output. (As shown in Figure 3.)

Unlike 2D convolution operation, the depth of the 3D convolution filters is less than the depth of corresponding input volume. The feature maps obtained by the filter $k^{(c)}$ in the c^{th} layer are given by:

$$T_{d,k}^{(c)} = T_d^{(c-1)} - k_d^{(c)} + 1 \quad (8)$$

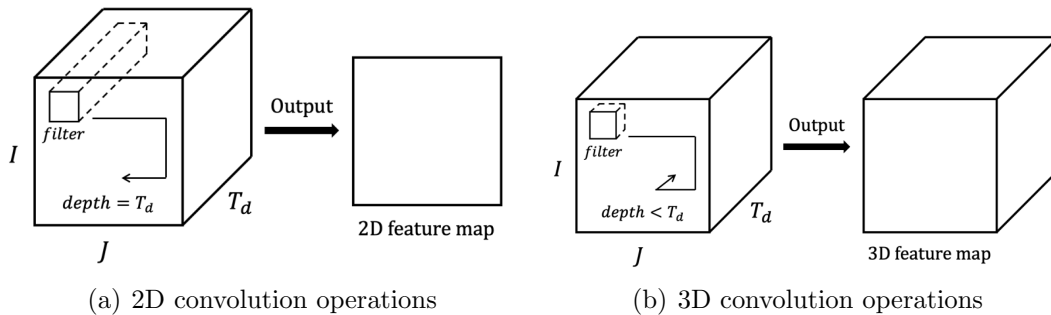


Figure 3: The difference between 2D and 3D convolution operations.

$$X_k^{(c)} = \text{ReLU}(W_k^{(c)} * X^{(c-1)} + b_k^{(c)}), X_k^{(c)} \in \mathbb{R}^{I \times J \times T_{d,k}^{(c)}} \quad (9)$$

where $W_k^{(c)}$ is the parameter matrices of filter k connected to the feature maps in the previous layer, $k_d^{(c)}$ is the depth and $b_k^{(c)}$ is intercept parameter. The asterisk denotes the convolutional operator and f is an activation function, convolving each filter across the width, height and depth of the input volume and computing dot products between the entries of the filter and input at any position. Each filter produces a separate 3D feature maps $X_k^{(c)}$, where the dimension of the depth of $X_k^{(c)}$ is $T_{d,k}^{(c)}$ obtained by valid convolution with stride 1 on previous layer with depth of $T_d^{(c-1)}$. Thus, finally the filter will be able to get access to all the information across the temporal dimension after a certain number of convolutions, depending on T_d . In the 3D convolutional layers, the filters have shared weights and the ReLU function is used (Krizhevsky, 2012).

After the 3D convolutional layers, we use a few 2D convolutional layers to further extract spatiotemporal features from low to high level and local to global. Stacking convolutional layers with tiny filters as opposed to having one convolutional layer with big filters allows us to express more powerful features of the input, and with fewer parameters.

3.3. Locally connected convolutional layer

The setting of parameter sharing in standard convolutional layers assumes local features. For example, if a horizontal boundary in some parts of the image is regarded important, then it will be equally useful in other places. However, the parameter sharing assumption may not be applicable for demand forecasting problems as the local features vary from region to region. For example, radial cities often have a typical central structure, and it is clearly inappropriate to use the same parameters to predict the demands for both the central and marginal areas of the city.

Hence, we relax the assumption of parameter sharing in standard convolution layers by using locally connected layers (without weight sharing) to obtain the final predictions. Like a standard convolutional layer, they apply a filter bank, except that every location in the feature maps is learnt by a different set of filters. As shown in Figure 4(a), in locally connected convolutional layers, the kernels in different spatial locations have different parameters. Compared with fully connected layers (Figure 4(b)) or standard convolutional layers, locally connected convolution layers can simultaneously maintain local statistics and spatial coordinates.

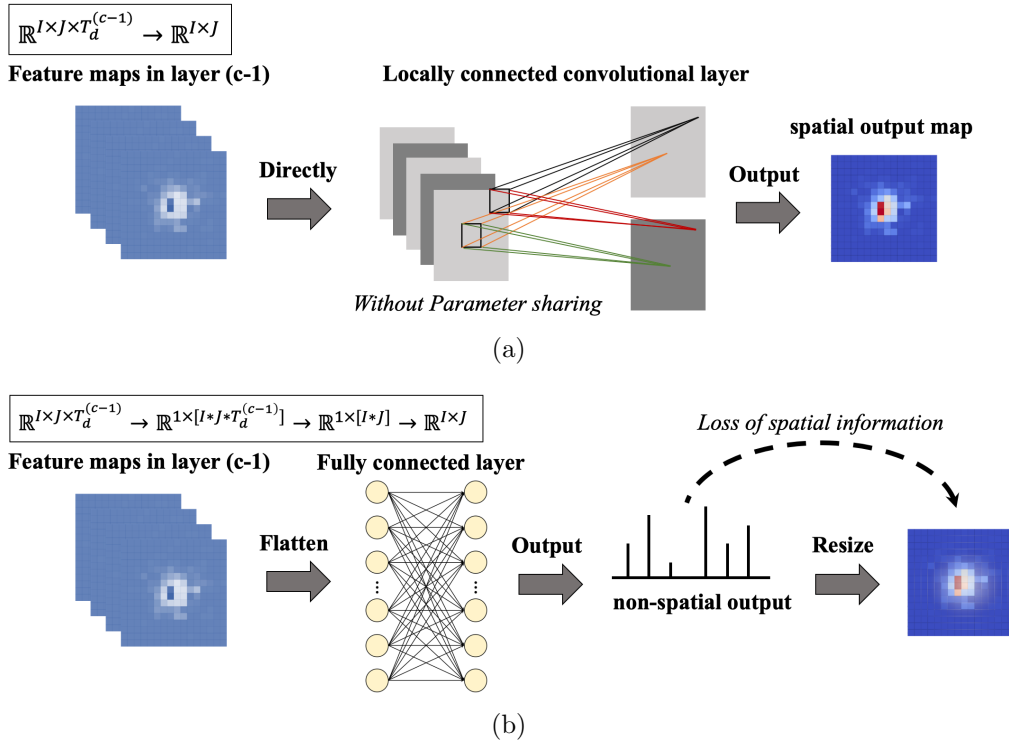


Figure 4: Schematic diagram showing the transformation of fully connected layers into locally connected convolution layers to output a heatmap.

3.4. Objective function

The LC-ST-FCN model can be trained by minimizing the mean squared error between the estimated demand \hat{X}_t and real demand X_t . The objective function is shown in Eq.(10), where w and b are both learnable parameters. Algorithm 1 outlines the LC-ST-FCN training process, where the adaptive sub-gradient method is adopted for model training.

$$\min_{w,b} \|X_t - \hat{X}_t\|_2^2 \quad (10)$$

4. Experiments

We perform experiments using a dataset from DiDiChuxing (<https://gaia.didichuxing.com>), which is the largest ride-sourcing service platform in China. The dataset includes customer requests in Chengdu, China, containing the request time, longitude, and latitude. After the raw data is cleaned, the dataset contained 7,031,022 requests within 103.85-104.30 longitude to the east and 30.48-30.87 latitude to the north are used in our experiments. All the requests are partitioned into 10-minute time intervals, and the investigated area is partitioned into 16×16 grids. Considering the periodicity of the data (see Figure 5), we select the first three weeks of the dataset as a training set D_{train} , and the remaining nine days as an independent testing set D_{test} .

Because of the inherent periodicity of urban activity, before training we use the additive model to decompose the total demand data X_t^{all} by time horizon length, L . After testing, we find that $L = 144$ (a day) or 1008 (a week) yields better decomposition results than others.

Algorithm 1 LC-ST-FCN training algorithm.

Input: Historical demand of each region: X_0, X_1, \dots, X_n ; Lengths of input data sequence: T_d ;

Lengths of recent and period sequence: T_{recent}, T_{period} ; Lengths of period interval: L .

Output: Learned LC-ST-FCN model.

```

1: // construct training instance:
2:  $D \leftarrow \emptyset$ 
3: for all available time interval  $t(1 \leq t \leq n)$  do
4:    $X_{recent} = [X_{t-1}, \dots, X_{t-T_{recent}}]$ 
5:    $X_{period} = [X_{t-L-1}, \dots, X_{t-L-T_{period}}]$ 
6:   //  $X_t$  is the target at time  $t$ 
7:   put a training instance  $(\{X_{recent}, X_{period}\}, X_t)$  into  $D$ 
8: end for
9: // Training:
10: repeat
11:   Initialize the biases and weights at each layer;
12:   Sample minibatch from  $D$  randomly;
13:   if in 2D or 3D convolution layers then
14:     for filters  $k \in K$  do
15:       // Parameter sharing
16:        $k \leftarrow$  learnable parameters  $w_k, b_k$ 
17:     end for
18:   end if
19:   if in locally connected convolution layers then
20:     for filters  $k \in K$  do
21:       // Without parameter sharing
22:        $k \leftarrow$  learnable parameters  $w_k^{loc}, b_k^{loc}$ 
23:     end for
24:   end if
25:   Calculate the stochastic gradient by minimizing the objective function
26:   shown in Eq.(10);
27:   Update the parameters via back-propagation;
28: until stopping criteria are met

```

As shown in Figure 6, for $L = 1008$, X_t^{tre} is almost linear and the distribution of residual terms has smaller variance than that for $L = 144$. Hence, we select $L = 1008$ to construct our training 3D tensor for training. In order to illustrate the effectiveness of 3D convolution for learning time dependence (short-term and periodic), we compare our results with the traditional difference method (Brockwell and Davis, 2015). In the experiment, we set $T_{recent} = T_{period} = 10$. Correspondingly, we use four 3D convolutional layers with filter depth $k_d = 3, 5, 7, 8$ to extract the spatiotemporal information of input. And the number of standard and locally-connected convolutional layers are 4 and 2.

To evaluate the performance of the LC-ST-FCN model, we select a bunch of different models as benchmarks, where all the models are trained and validated with the same training set and test set:

- (1) LC-FCN: Variant of the LC-ST-FCN model, where the 2D convolutional layer are applied to the input to generate feature maps instead of 3D convolution layer. So, the temporal dimension of input is collapsed after the first 2D convolutional layer.
- (2) FCN: Variant of the LC-FCN model, where the last two layers are standard 2D convolu-

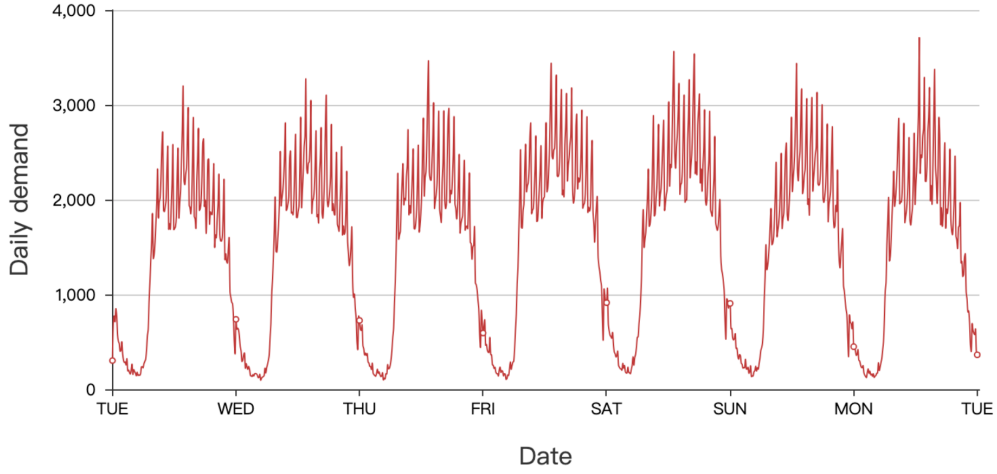
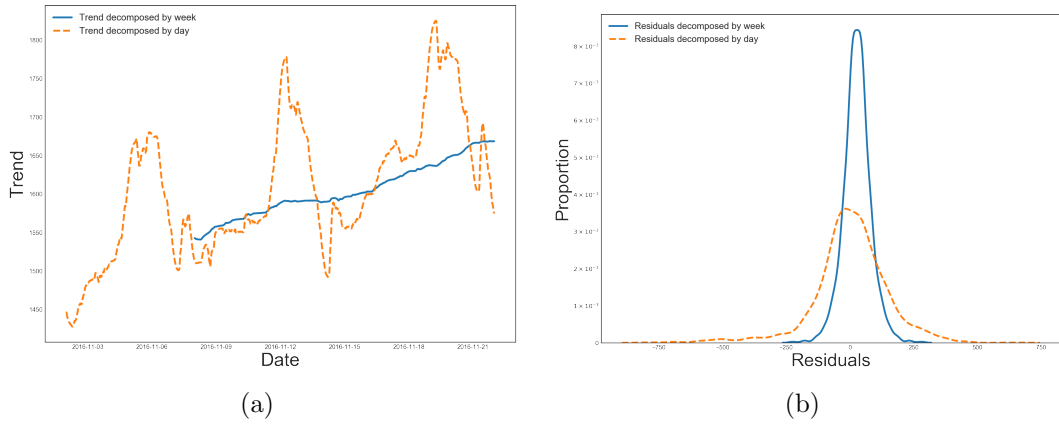


Figure 5: Daily demand in the first week of November 2016 (all regions).



(a)

(b)

Figure 6: Schematic diagram showing the transformation of fully connected layers into locally connected convolution layers to output a heatmap.

tional layers (weight sharing), while the other parts of the structure remain the same.

- (3) LC-ST-FCN (diff): Variant of the LC-ST-FCN model, where the difference method is used to generate input data.
- (4) CNN: The last two layers are fully connected layers, while the other parts of the structure are the same as FCN.
- (5) Conv-LSTM: Conv-LSTM layers (Xingjian and Woo, 2015) are used instead of convolution layers in FCN. Conv-LSTM structure can simultaneously learn spatial correlation and time dependence.
- (6) ANN (artificial neural network): Since different regions of a city have different local statistics, it is difficult to achieve effective prediction for all regions using a single ANN. Hence, we use a unique ANN for training and prediction in each grid region, resulting in a total of 256 ANNs that are trained. The input of 1-dimension time series data has a size of $1 \times 1 \times 20$, where 20 is the length of the temporal dimension.
- (7) Additive model: As for ANN, 256 independent addition models are used to obtain final prediction results for each region.
- (8) ARIMA: As ARIMA requires the stability and randomness of data, in our experiments, it is only used to generate predictions in regions that meet the requirements of stationarity and randomness.

4.1. Model comparison with arithmetic-mean-based metrics

We first evaluate our model by the root mean squared error (RMSE), normalized root mean squared error (NRMSE), mean absolute percentage error (MAPE), and the modified MAPE methods according to a previous study (Chen and Li, 2018; Moreira-Matias et al., 2013), which are defined as follows:

$$RMSE_{i,j} = \sqrt{\frac{1}{n} \sum_{r=1}^n (x_t^{i,j} - \hat{x}_t^{i,j})^2} \quad (11)$$

$$NRMSE_{i,j} = \sqrt{\frac{\sum_{r=1}^n (x_t^{i,j} - \hat{x}_t^{i,j})^2}{\sum_{r=1}^n (x_t^{i,j})^2}} \quad (12)$$

$$MAPE_{i,j} = \frac{1}{n} \sum_{r=1}^n \frac{|x_t^{i,j} - \hat{x}_t^{i,j}|}{x_t^{i,j} + c} \quad (13)$$

$$sMAPE1_{i,j} = \frac{1}{n} \sum_{r=1}^n \frac{|x_t^{i,j} - \hat{x}_t^{i,j}|}{x_t^{i,j} + \hat{x}_t^{i,j} + c} \quad (14)$$

$$sMAPE2_{i,j} = \frac{\sum_{r=1}^n |x_t^{i,j} - \hat{x}_t^{i,j}|}{\sum_{r=1}^n |x_t^{i,j} + \hat{x}_t^{i,j}|} \quad (15)$$

Here, n is the number of all predicted values, $x_t^{i,j}$ and $\hat{x}_t^{i,j}$ are the ground truth and predicted value of demand in region (i, j) at time interval t , respectively, while c in Eq.(13) and (14) are set to 1.

Table 1 compares the predictive performances of the seven models on the test dataset. The numbers in the parentheses beside each value are the ranking of the predictive performance for the corresponding measurements. The results predicted by ARIMA are not included in the comparison range in Table 1 due to the requirement of stationarity and randomness of the data.

Table 1: Comparison of the predictive performance of the various models using the same test dataset.

| Model | RMSE | NRMSE (%) | MAPE (%) | sMAPE1 (%) | sMAPE2 (%) |
|------------------|----------|------------|-----------|------------|------------|
| LC-ST-FCN | 1.67 (1) | 75.38 (2) | 22.40 (1) | 13.31 (3) | 13.85 (1) |
| LC-FCN | 1.69 (2) | 75.28 (1) | 22.98 (2) | 13.45 (4) | 13.85 (1) |
| FCN | 1.78 (3) | 99.67 (5) | 27.36 (7) | 15.91 (7) | 16.93 (7) |
| CNN | 1.82 (4) | 104.62 (6) | 25.78 (6) | 15.09 (6) | 16.11 (5) |
| Additive model | 1.86 (5) | 91.24 (4) | 24.78 (4) | 13.21 (2) | 14.96 (4) |
| Conv-LSTM | 1.95 (6) | 131.02 (8) | 28.69 (8) | 17.04 (8) | 18.74 (8) |
| ANN | 2.04 (7) | 76.92 (3) | 24.43 (3) | 14.23 (5) | 14.53 (3) |
| LC-ST-FCN (diff) | 2.17 (8) | 105.53 (7) | 25.72 (5) | 13.19 (1) | 16.11 (5) |

As shown by Table 1, LC-ST-FCN model obtains the best results on RMSE, MAPE and sMAPE2. Generally, LC-ST-FCN has better predictive performance than LC-FCN, which indicates that the 3D convolution operations capture the spatiotemporal information better

than 2D ones. Compared with LC-FCN, FCN and CNN, the predictive performance of LC-FCN is significantly improved by simply replacing the last two standard convolutional layers or fully connected layers with locally connected convolutional layers. Which implies that the local-to-global-to-local architectures have excellent adaptability to the complex and changeable demand patterns of different regions in a city.

However, further comparison of the models is difficult due to the inconsistencies among the evaluation metrics. We observe the following interesting phenomena in Table 1. The RMSE of CNN is less than that of the additive model, while all the relative errors (i.e. NRMSE and the others) are greater than that of the additive model. The same situation occurs in the comparison of FCN and the additive model, CNN and ANN, FCN and ANN, and Conv-LSTM and ANN. Moreover, the contradictions among percentage error metrics are even more obvious. In general, relative errors are expressed as a ratio (unitless number), which can eliminate the influence of scale and better reflect the credibility of the measurement. However, when the absolute error and relative error are inconsistent in the evaluation results, it is difficult to effectively judge which model is superior. Such inconsistency is caused by the unbalanced demands of the regions. Thus, it is necessary to modify the evaluation criteria as well as the model structure, So that the evaluations of different models can be consistent.

4.2. Issues in model evaluation

Three issues will affect the effectiveness of the model evaluation: (1) the demand uncertainty; (2) the demand level; and (3) the demand distribution. We analyze each issue below.

(1) Demand uncertainty

In the literature, the uncertainty of data is seldom considered when training DL models. Especially, in short-term demand forecasting problems, such uncertainties significantly impact the model predictive performance. The CNN models do not output probability distributions. So attempting to extract the outcome of a sequence of a random time series data simply transfers the randomness from the inputs to the outputs. In each grid region, the historical observations $\{x_t^{i,j} \mid t = 0, \dots, n - 1; (i, j) \in (I, J)\}$ constitute an independent time series dataset. To extract the demand uncertainty, we use the *LjungBox test* to assess the randomness of $x_t^{i,j}$. If the p value of the test is greater than 0.05, $x_t^{i,j}$ is considered a random sequence. Based on the results of the *LjungBox test*, the set of all regions, G , can be divided into a non-random sequence set G_1 and random sequence set G_2 , where $G_1 \cap G_2 = \emptyset$ and $G_1 \cup G_2 = G$. In this case, for the total 256 grid regions, G_1 contains only 56 regions ($G_1/G = 21.87\%$), but accounts for 80.88% of the total demand, while G_2 contains 200 regions ($G_2/G = 78.13\%$), but accounts for only 19.12% of the total demand. As shown in Figure 7, we choose a group of regions adjacent to each other in latitude and acrossing the city center, and compare the frequency distributions of real and predicted data within the test data set. The difference between the two distributions is usually measured by the Kullback-Leibler (KL) divergence (Kullback and Leibler, 1951). We can easily observe that the gap between the two distributions is bigger for the regions in G_2 (regions 8-5, 8-6, 8-11, 8-12, 8-13) rather than G_1 , which implies that the model encounters greater difficulties in learning the distribution of G_2 regions with higher uncertainty. Therefore, it is necessary to treat the two different types of regions separately in the model evaluation.

(2) Demand level

The percentage error measurements should not be used to evaluate the overall performance of the model, since they are very sensitive to the level of absolute demand. For example, we

compare the prediction results of the additive model for regions 10-2 and 8-8, as shown in Table 2 and Figure 8. In Table 2, the model has a better performance for region 10-2 in almost all the percentage error measurements. However, Figure 10 indicates an opposite conclusion that the prediction for region 8-8 is better, since the pattern of demand oscillation is well learned by the model.

(3) Demand distribution

The Gini coefficient is most often used to measure how far a distribution deviates from a totally equal distribution. We calculate the Gini coefficient of the order demand distribution based on a Lorenz curve, which plots the proportion of the total demand of the city as a function of the cumulative share of the regional demand (as shown in Figure 9). The $y = x$ line represents perfect equality of demand. Hence, the Gini coefficient is the ratio of the area that lies between the lines of equality and the Lorenz curve (marked as A in the figure) to the total area under the line of equality (A + B in the figure). As a result of the variety of urban geography and layout, the Gini coefficient of our demand dataset is around 0.89, indicating extreme spatial unbalance of demand.

When the regional demand is highly unbalanced in a city, the evaluation results obtained by the arithmetic-mean-based methods are affected by the extreme values. The inherent averaging effect hides the complexity and heterogeneity behind the prediction results.

We sort all regions in increasing order in terms of demand level and calculate the cumulative moving average of the percentage errors of each model, as shown in Figure 10. We can observe that the curve is almost flat after the demand is larger than 25. This implies that the percentage measurement is determined mainly by the low demand regions, which occupy the majority of the prediction area. This may not be reasonable since the regions with large demand should be paid more attention.

From another point of view, when we increase the grid size from 16×16 to 64×64 with the same LC-ST-FCN structure, the prediction resolution is reduced. However, Table 3 shows a significant improvement for all the arithmetic-mean-based metrics, which indicates that the such measurements cannot objectively reflect the prediction ability of the model.

Table 2: Prediction error of region 10-2 and 8-8 (Additive model).

| | RMSE | NRMSE (%) | MAPE (%) | sMAPE1 (%) | sMAPE2 (%) |
|---------------|-------|-----------|----------|------------|------------|
| Region (10-2) | 0.15 | 118.29 | 1.79 | 1.42 | 2.34 |
| Region (8-8) | 23.06 | 9.13 | 17.90 | 7.27 | 4.08 |

Table 3: Prediction errors of the LC-ST-FCN model with different grid sizes.

| Grid size | RMSE | NRMSE (%) | MAPE (%) | sMAPE1 (%) | sMAPE2 (%) |
|----------------|------|-----------|----------|------------|------------|
| 16×16 | 1.67 | 75.38 | 22.40 | 13.31 | 13.85 |
| 64×64 | 0.35 | 62.5 | 5.83 | 3.77 | 5.37 |

4.3. Model comparison with weighted-arithmetic-based metrics

In order to address the above issues, we propose weighted-arithmetic-based metrics instead of the widely used arithmetic-mean-based metrics. The weight α_{ij} is obtained by calculating

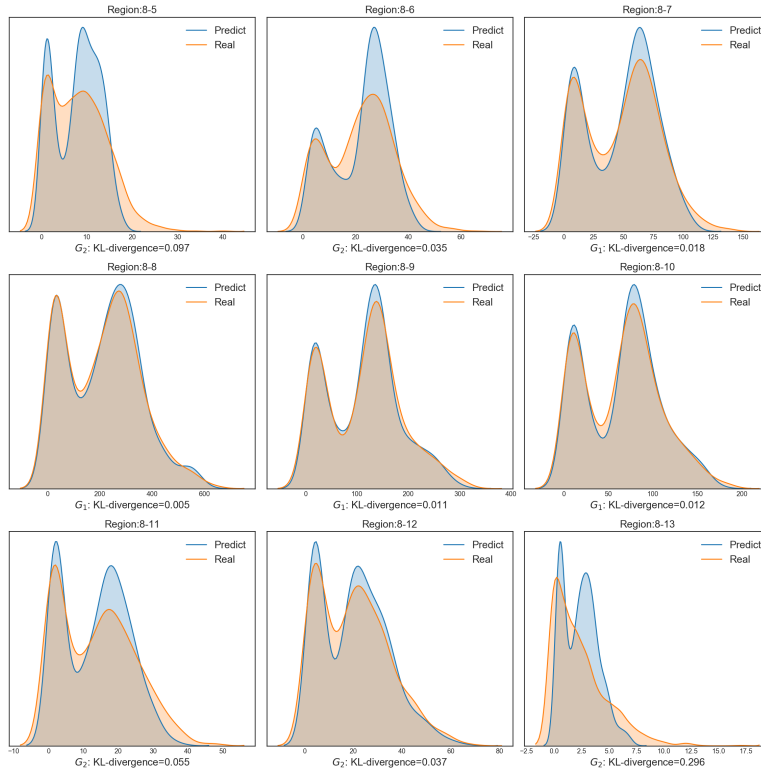


Figure 7: Frequency distribution of adjacent regions (from 8-5 to 8-13).

the ratio of the regional demand to total demand for the training set D_{train} . All the new metrics are shown in Table 4.

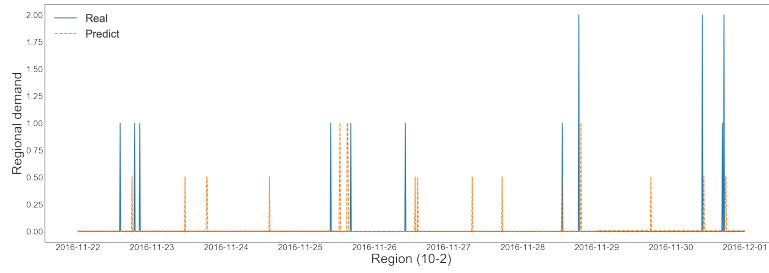
$$\alpha_{ij} = \frac{\sum_{t \in D_{train}} x_t^{i,j}}{\sum_{t \in D_{train}} \sum_{i,j \in I,J} x_t^{i,j}} \quad (16)$$

Table 4: The weighted-arithmetic-based metrics.

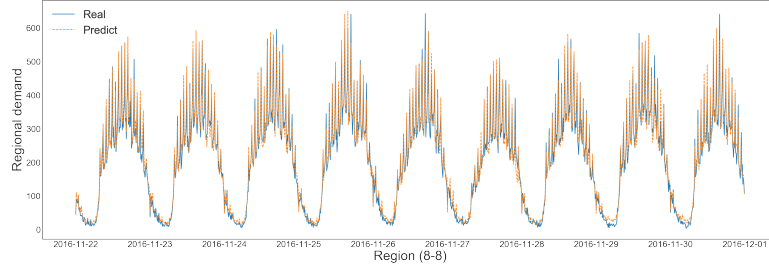
| Arithmetic-mean-based metrics | Weighted-arithmetic-based metrics |
|---|---|
| $NRMSE = \frac{1}{IJ} \sum_{i,j \in I,J} NRMSE_{i,j}$ | $W_NRMSE = \sum_{i,j \in I,J} \alpha_{ij} NRMSE_{i,j}$ |
| $MAPE = \frac{1}{IJ} \sum_{i,j \in I,J} MAPE_{i,j}$ | $W_MAPE = \sum_{i,j \in I,J} \alpha_{ij} MAPE_{i,j}$ |
| $sMAPE1 = \frac{1}{IJ} \sum_{i,j \in I,J} sMAPE1_{i,j}$ | $W_sMAPE1 = \sum_{i,j \in I,J} \alpha_{ij} sMAPE1_{i,j}$ |
| $sMAPE2 = \frac{1}{IJ} \sum_{i,j \in I,J} sMAPE2_{i,j}$ | $W_sMAPE2 = \sum_{i,j \in I,J} \alpha_{ij} sMAPE2_{i,j}$ |

Figure 10 shows the difference between the two kinds of metrics. It is obvious that the regions with higher demands now contribute more in the weighted-arithmetic-based metrics, which might be more preferable for the ride-sourcing platform, since higher priority should be given to regions with higher demand to guarantee the system efficiency. Moreover, the weighted arithmetic is less sensitive to the grid size as shown in Table 5.

The prediction errors calculated based on weighted-arithmetic metrics are shown in Table 6. Now the predictive performance rankings of the models under most metrics are consistent, except for W_MAPE. Under weighted-arithmetic metrics, the LC-ST-FCN proposed in this



(a)



(b)

Figure 8: Prediction results for region 10-2 and 8-8 (Additive model).

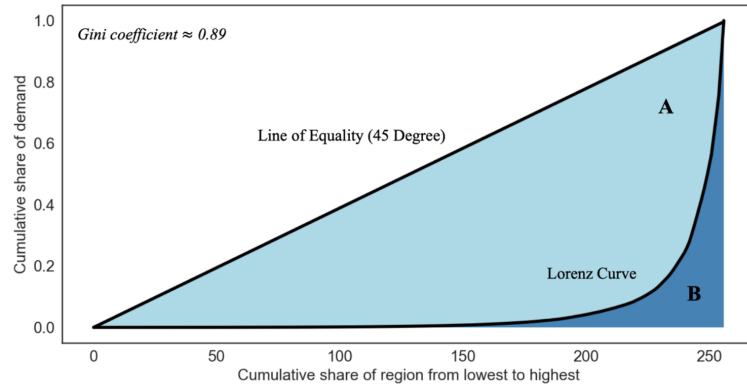


Figure 9: Gini coefficient of grid regions in the city.

study outperforms all the other benchmark models in all the five metrics. There are some interesting observations below:

i) In terms of predictive performance, $LC-ST-FCN > LC-FCN > FCN$, which indicates that 3D convolutions are more suitable for spatiotemporal feature learning compared to 2D convolutions; And the locally connected convolutional layers can deal with the impact of local statistical differences well, better than standard convolutional layers. The LC-ST-FCN, LC-FCN and FCN are the top three ranked models. That may be due to the fully convolutional architecture of them, which can help maintain the spatial coordinates of the input and avoid losing spatial information between layers.

ii) In terms of predictive performance, $FCN > CNN$. The only difference between the two structures is the last two layers. FCN and CNN use standard convolution layers, and fully connected layers, respectively. In our experiments, the ratio between the total numbers of parameters of the last two layers for the two models are nearly 1:8000. One of the reasons why FCN is superior to CNN might be that the fully connected layer in CNN is affected by a very large patch of the input and learning the optimal combination of parameters for numerous neurons is difficult.

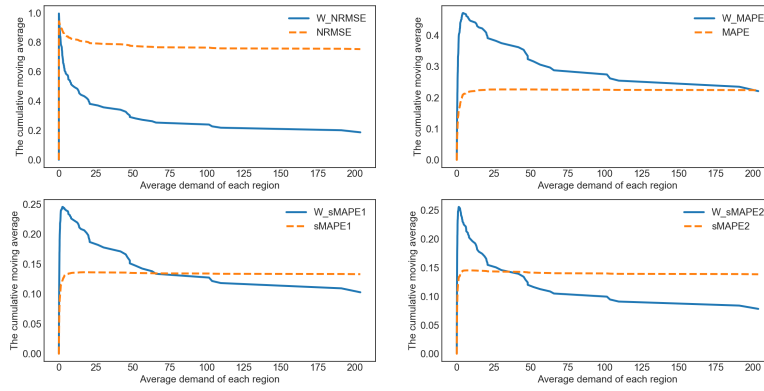


Figure 10: Comparison of the weighted and non-weighted evaluation functions.

iii) In terms of predictive performance, LC-ST-FCN > LC-ST-FCN (diff). The good predictive performance of additive model demonstrates that the trend and periodicity of demand data play an important role in demand forecasting. Both LC-ST-FCN (diff) and LC-ST-FCN can learn from these information, yet the results show that the 3D convolution operation is more powerful in feature extraction than difference method.

In order to further compare the predictive performance of each model in regions with different levels of uncertainty, we calculated the evaluation metrics for both G_1 and G_2 (Table 7). It can be observed that for all the models, the weighted percentage errors for G_2 are nearly doubled, which indicates that uncertainties in the time series data can greatly reduce the models' prediction ability.

Table 5: Prediction error of the LC-ST-FCN model for different grid sizes using the weighted method.

| Grid size | RMSE | W_NRMSE (%) | W_MAPE (%) | W_sMAPE1 (%) | W_sMAPE2 (%) |
|----------------|------|-------------|------------|--------------|--------------|
| 16×16 | 1.67 | 18.76 | 22.09 | 10.28 | 7.83 |
| 64×64 | 0.35 | 47.04 | 37.16 | 18.53 | 17.63 |

Table 6: Predictive performance comparison (weighted).

| Model | RMSE | W_NRMSE (%) | W_MAPE (%) | W_sMAPE1 (%) | W_sMAPE2 (%) |
|------------------|----------|-------------|------------|--------------|--------------|
| LC-ST-FCN | 1.67 (1) | 18.76 (1) | 22.09 (1) | 10.28 (1) | 7.83 (1) |
| LC-FCN | 1.69 (2) | 19.09 (2) | 23.39 (2) | 10.61 (2) | 7.96 (2) |
| FCN | 1.78 (3) | 19.80 (3) | 23.84 (3) | 10.88 (3) | 8.24 (3) |
| CNN | 1.82 (4) | 20.41 (4) | 24.43 (5) | 11.02 (4) | 8.45 (4) |
| Additive model | 1.86 (5) | 20.77 (5) | 26.99 (6) | 11.56 (5) | 8.63 (5) |
| Conv-LSTM | 1.95 (6) | 21.61 (6) | 24.32 (4) | 11.95 (6) | 9.16 (6) |
| ANN | 2.04 (7) | 23.42 (7) | 28.57 (8) | 12.79 (7) | 9.82 (7) |
| LC-ST-FCN (diff) | 2.17 (8) | 24.32 (8) | 27.02 (7) | 12.92 (8) | 9.96 (8) |

Table 7: Predictive performance of G_1 and G_2 (weighted method).

| Model | RMSE | W_NRMSE (%) | W_MAPE (%) | W_sMAPE1 (%) | W_sMAPE2 (%) |
|-----------------------|-----------|-------------|-------------|--------------|--------------|
| regions (G_1/G_2) | | | | | |
| LC-ST-FCN | 4.35/0.92 | 14.40/37.21 | 18.38/37.79 | 8.45/18.04 | 6.12/15.05 |
| LC-FCN | 4.47/0.91 | 14.82/37.14 | 19.71/38.91 | 8.80/18.23 | 6.29/15.04 |
| FCN | 4.57/1.01 | 15.09/39.72 | 19.77/41.01 | 8.95/19.04 | 6.42/15.93 |
| CNN | 4.83/0.98 | 16.01/39.01 | 20.76/39.99 | 9.24/18.57 | 6.76/15.63 |
| Additive model | 4.75/1.05 | 15.68/42.29 | 23.21/42.99 | 9.69/19.51 | 6.72/16.7 |
| Conv-LSTM | 5.14/1.06 | 16.97/41.23 | 20.72/39.55 | 10.15/19.59 | 7.36/16.77 |
| ANN | 5.79/0.99 | 19.35/40.65 | 24.64/45.18 | 11.06/20.07 | 8.19/16.7 |
| LC-ST-FCN (diff) | 5.60/1.21 | 18.51/48.92 | 22.78/44.99 | 10.98/21.15 | 7.85/18.9 |
| ARIMA | 5.52/- | 18.23/- | 22.09/- | 10.75/- | 7.74/- |

5. Conclusions

CNN has been demonstrated as an effective tool for learning information with spatial structure, which has led to breakthroughs in almost all machine learning tasks. In this paper, a fusion convolutional model, LC-ST-FCN, is established for demand forecasting of ride-sourcing services. New model structure and evaluation metrics are developed to deal with the unique characteristics of ride-sourcing services. A real dataset from DiDiChuxing platform is used for model evaluation and comparison. In the experiments, our model outperforms all the benchmark models in terms of all the weighted-arithmetic-based metrics and most of the arithmetic-mean-based metrics. The weighted-arithmetic-based metrics show better consistency in performance evaluation than the arithmetic-mean-based metrics, because they take demand level and unbalanced demand distribution into consideration. Moreover, we show that prediction results can be greatly affected by the local statistics, since in our experiments, the percentage errors in regions with high uncertainty are nearly twice of those in regions with low uncertainty. In this paper, the training data of our proposed model is generated by grid-based partition, which is carried out independently of the model training. In the future work, we expect to explore a learnable partition algorithm which has the ability of automatic region partition by learning the demand statistics of ride-sourcing service platforms.

Acknowledgement

The dataset used in this paper comes from DiDiChuxing. The work described in this paper was supported by the National Key Research and Development Program of China (2018YFB1600902) and the National Natural Science Foundation of China (71622007, 71861167001, 71725001).

References

References

- Auer, M., Rehborn, H., Molzahn, S.-E., Koller, M., 2017. Traffic services for vehicles: the process from receiving raw probe data to space-time diagrams and the resulting traffic service. *Frontiers of Engineering Management*. 4 (4), 490–497.
- Brockwell, P. J., Davis, R. A., 2015. *Time Series: Theory and Methods*. Springer-Verlag.

- Chang, H. W., Tai, Y. C., Hsu, Y. J., 2009. Context-aware taxi demand hotspots prediction. *International Journal of Business Intelligence and Data Mining*. 5 (1), 3–18.
- Chen, Xiqun Michael, C. C. L. N., Li, L., 2018. Spatial visitation prediction of on-demand ride services using the scaling law. *Physica A: Statistical Mechanics and its Applications*. 508, 84–94.
- Chen, X., Zahiri, M., Zhang, S., 2017a. Understanding ridesplitting behavior of on-demand ride services: An ensemble learning approach. *Transportation Research Part C: Emerging Technologies*. 76, 51–70.
- Chen, X. M., Chen, X., Zheng, H., Chen, C., 2017b. Understanding network travel time reliability with on-demand ride service data. *Frontiers of Engineering Management*. 4 (4), 388–398.
- Deng, Z., Ji, M., 2011. Spatiotemporal structure of taxi services in shanghai: Using exploratory spatial data analysis. In: *2011 19th International Conference on Geoinformatics*. pp. 1–5.
- Dong, Y., Wang, S., Li, L., Zhang, Z., 2018. An empirical study on travel patterns of internet based ride-sharing. *Transportation Research Part C: Emerging Technologies*. 86, 1–22.
- Gregor, K., Lecun, Y., 2010. Emergence of complex-like cells in a temporal product network with local receptive fields. *arXiv:1006.0448*.
- Hara, K., Kataoka, H., Satoh, Y., 2017. Learning spatio-temporal features with 3d residual networks for action recognition. In: *Proceedings of the IEEE international conference on computer vision*. pp. 3154–3160.
- Huang, G. B., Lee, H., Learned-Miller, E., 2012. Learning hierarchical representations for face verification with convolutional deep belief networks. In: *2012 IEEE Conference on Computer Vision and Pattern Recognition*. pp. 2518–2525.
- Huang, W., Song, G., Hong, H., Xie, K., 2014. Deep architecture for traffic flow prediction: Deep belief networks with multitask learning. *IEEE: Transactions on Intelligent Transportation Systems*. 15 (5), 2191–2201.
- Jessica Christian, S. E., 2018. Study: Half of sfs increase in traffic congestion due to uber, lyft. <http://www.sfexaminer.com/study-half-sfs-increase-traffic-congestion-due-uber-lyft/>.
- Kaltenbrunner, A., Meza, R., Grivolla, J., Codina, J., Banchs, R., 2010. Urban cycles and mobility patterns: Exploring and predicting trends in a bicycle-based public transport system. *Pervasive and Mobile Computing*. 6 (4), 455–466.
- Karpathy, A., Toderici, G., Shetty, S., Leung, T., Sukthankar, R., Fei-Fei, L., 2014. Large-scale video classification with convolutional neural networks. In: *Proceedings of the IEEE conference on Computer Vision and Pattern Recognition*. pp. 1725–1732.
- Ke, J., Zheng, H., Yang, H., Chen, X., 2017. Short-term forecasting of passenger demand under on-demand ride services: A spatio-temporal deep learning approach. *Transportation Research Part C: Emerging Technologies*. 85, 591–608.
- Krizhevsky, A., S. I. H. G., 2012. Imagenet classification with deep convolutional neural networks. In: *Advances in Neural Information Processing Systems*. pp. 1097–1105.
- Kullback, S., Leibler, R. A., 1951. On information and sufficiency. *Annals of Mathematical Statistics*. 22 (1), 79–86.

- Lecun, Y., Bengio, Y., Hinton, G., 2015. Deep learning. *Nature*. 521 (7553), 436.
- LeCun, Y., Boser, B., Denker, J. S., Henderson, D., Howard, R. E., Hubbard, W., Jackel, L. D., 1989. Backpropagation applied to handwritten zip code recognition. *Neural computation*. 1 (4), 541–551.
- Ma, X., Dai, Z., He, Z., Ma, J., Wang, Y., Wang, Y., 2017. Learning traffic as images: a deep convolutional neural network for large-scale transportation network speed prediction. *Sensors*. 17 (4), 818.
- Ma, X., Yu, H., Wang, Y., Wang, Y., 2015. Large-scale transportation network congestion evolution prediction using deep learning theory. *Plos One*. 10 (3), e0119044.
- Moreira-Matias, L., Gama, J., Ferreira, M., Mendes-Moreira, J., Damas, L., 2013. Predicting taxipassenger demand using streaming data. *IEEE: Transactions on Intelligent Transportation Systems*. 14 (3), 1393–1402.
- Shelhamer, E., Long, J., Darrell, T., 2014. Fully convolutional networks for semantic segmentation. *IEEE: Transactions on Pattern Analysis and Machine Intelligence*. 39 (4), 640–651.
- Shuiwang, J., Ming, Y., Kai, Y., 2013. 3d convolutional neural networks for human action recognition. *IEEE: Transactions on Pattern Analysis and Machine Intelligence*. 35 (1), 221–231.
- Simonyan, K., Zisserman, A., 2014a. Two-stream convolutional networks for action recognition in videos. pp. 568–576.
- Simonyan, K., Zisserman, A., 2014b. Very deep convolutional networks for large-scale image recognition. arXiv:1409.1556.
- Szegedy, C., Liu, W., Jia, Y., Sermanet, P., Reed, S., Anguelov, D., Erhan, D., Vanhoucke, V., Rabinovich, A., 2015. Going deeper with convolutions. In: *Proceedings of the IEEE conference on computer vision and pattern recognition*. pp. 1–9.
- Taigman, Y., Yang, M., Ranzato, M., Wolf, L., 2014. Deepface: Closing the gap to human-level performance in face verification. In: *Proceedings of the IEEE conference on computer vision and pattern recognition*. pp. 1701–1708.
- Tran, D., Bourdev, L., Fergus, R., Torresani, L., Paluri, M., 2015. Learning spatiotemporal features with 3d convolutional networks. In: *Proceedings of the IEEE international conference on computer vision*. pp. 4489–4497.
- Vazifeh, M. M., Santi, P., Resta, G., Strogatz, S. H., Ratti, C., 2018. Addressing the minimum fleet problem in on-demand urban mobility. *Nature*. 557 (7706), 534–538.
- Xingjian, S.H.I., C. Z. W. H. Y. D. W. W., Woo, W., 2015. Convolutional lstm network: A machine learning approach for precipitation nowcasting. In: *Advances in neural information processing systems*. pp. 802–810.
- Yao, H., Wu, F., Ke, J., Tang, X., Jia, Y., Lu, S., Gong, P., Ye, J., Li, Z., 2018. Deep multi-view spatial-temporal network for taxi demand prediction. In: *Thirty-Second AAAI Conference on Artificial Intelligence*.
- Yu, R., Li, Y., Shahabi, C., Demiryurek, U., Liu, Y., 2017. Deep learning: A generic approach for extreme condition traffic forecasting. In: *Proceedings of the 2017 SIAM International Conference on Data Mining*. pp. 777–785.

- Yuan, J., Zheng, Y., Zhang, L., Xie, X., Sun, G., 2011. Where to find my next passenger. In: Proceedings of the 13th international conference on Ubiquitous computing. pp. 109–118.
- Zhang, J., Zheng, Y., Qi, D., 2017. Deep spatio-temporal residual networks for citywide crowd flows prediction. In: Thirty-First AAAI Conference on Artificial Intelligence.
- Zhao, K., Khryashchev, D., Freire, J., Silva, C., Vo, H., 2016. Predicting taxi demand at high spatial resolution: Approaching the limit of predictability. In: 2016 IEEE International Conference on Big Data (Big Data). pp. 833–842.